J Mater Sci: Mater Med (2011) 22:1455–1464
DOI 10.1007/s10856-011-4324-5

Effects of thermal treatments on protein adsorption of Co–Cr–Mo ASTM-F75 alloys

L. A. Duncan · F. H. Labeed · M.-L. Abel · A. Kamali · J. F. Watts

Received: 17 March 2010 / Accepted: 16 April 2011 / Published online: 10 May 2011

Abstract Post-manufacturing thermal treatments are commonly employed in the production of hip replacements to reduce shrinkage voids which can occur in cast components. Several studies have investigated the consequences of these treatments upon the alloy microstructure and tribological properties but none have determined if there are any biological ramifications. In this study the adsorption of proteins from foetal bovine serum (FBS) on three Co–Cr–Mo ASTM-F75 alloy samples with different metallurgical histories, has been studied as a function of protein concentration. Adsorption isotherms have been plotted using the surface concentration of nitrogen as a diagnostic of protein uptake as measured by X-ray photoelectron spectroscopy. The data was a good fit to the Langmuir adsorption isotherm up to the concentration at which critical protein saturation occurred. Differences in protein adsorption on each alloy have been observed. This suggests that development of the tissue/implant interface, although similar, may differ between as-cast (AC) and heat treated samples.

L. A. Duncan · F. H. Labeed · M.-L. Abel · J. F. Watts (✉)
Faculty of Engineering and Physical Sciences, University of Surrey, Guildford, Surrey GU2 7XH, UK
e-mail: J.Watts@surrey.ac.uk

L. A. Duncan
e-mail: l.duncan@surrey.ac.uk

F. H. Labeed
e-mail: f.labeed@surrey.ac.uk

M.-L. Abel
e-mail: m.abel@surrey.ac.uk

A. Kamali
Implant Development Centre, Smith & Nephew Orthopaedics Ltd, Leamington Spa, Warwick CV31 3HL, UK
e-mail: amir.kamali@smith-nepthew.com

1 Introduction

Co–Cr–Mo alloys are one of the most commonly used materials for hip arthroplasty and are favoured for their desirable mechanical properties, corrosion resistance, wear resistance and biocompatibility. This alloy is used in a variety of conditions which are dependent upon the composition, manufacturing methods, and post-manufacturing thermal treatments [1]. High carbon AC Co–Cr–Mo alloys are biphasic containing a matrix phase rich in cobalt, chromium, and molybdenum and a carbide phase rich in chromium, molybdenum and carbon [2]. The AC alloy microstructure contains large blocky carbides and has an overall carbide volume fraction of ~5% [1, 3]. AC Co–Cr–Mo alloys may contain defects known as shrinkage voids which can reduce the overall mechanical properties of the material under certain loading conditions [1]. Thermal treatments such as hot isostatic pressing (HIP) and solution annealing (SA) have been employed to fully densify and therefore improve the mechanical properties of the alloy [1, 4]. In addition the post manufacturing thermal treatments render the alloy easier to machine [5].

The HIPing parameters of AC Co–Cr–Mo alloys subject the component to a temperature of 1,200°C for four hours in an inert atmosphere. The components are then quenched in argon at a rate of approximately 8–10°C per minute at an isostatic pressure of approximately 103 MPa [1, 2]. This process produces finer agglomerated and lamellar carbides with a reduced overall volume fraction (approximately 2.3% [1]) [5]. The procedure for SA of Co–Cr–Mo alloys is similar to that of HIPing however after heating for 4 h at 1,200°C the component is rapidly quenched to 800°C in less than 8 min (50°C per minute) [1, 2, 5]. The consequence of the rapid quenching restricts the reprecipitation

of the carbide phase dramatically reduces the overall volume fraction of the carbide phase [1, 2, 5].

Tribological studies have shown that lower levels of wear exhibited by AC Co–Cr–Mo alloys have been attributed to their higher overall volume fraction of carbides [1, 6]. Much work has been carried out to investigate the consequences of thermal treatments upon the mechanical/tribological characteristics of an alloy [1, 2, 7, 8], but little has been done to study what, if any, biological ramifications exist as a result of metallurgical conditions.

Materials interact with their environment through their interfaces. The development of the tissue/implant interface is crucial in determining the ultimate biological response to the implant [9]. It is widely acknowledged that one of the initial events that occurs when an implant is introduced into a patient is the adsorption of proteins from the surrounding blood and tissue fluids [9, 10]. As the tissue/implant interface develops, cells eventually reach the surface; at this time they are presented not with the surface of the implant but with a proteinaceous layer to which they bind via membrane receptors [11]. The type and conformation of the proteins will determine which cells bind to the site.

This study investigates the adsorption of proteins from foetal bovine serum (FBS) on a Co–Cr–Mo alloy manufactured to the following specifications stipulated in ASTM-F75. ASTM-F75 is a standard specification for Co–Cr–Mo surgical implant applications which, amongst other things, cover the alloy's composition (see Table 1). Three samples, each with a different post-manufacturing thermal history, have been used: AC, SA, and HIPSA.

Table 1 Chemical compositions as set out by ASTM-F75 98 and ISO 5832 Part 4

Element	Composition, % (Mass/mass)	
	Min	Max
Chromium	27	30
Molybdenum	5	7
Nickel	–	0.5
Iron	–	0.75
Carbon	–	0.35
Silicon	–	1
Manganese	–	1
Tungsten	–	0.2
Phosphorous	–	0.02
Sulfur	–	0.01
Nitrogen	–	0.25
Aluminium	–	0.1
Titanium	–	0.1
Boron	–	0.01
Cobalt	Balance	Balance

In the present study, the aim is to investigate the adsorption of proteins from FBS on Co–Cr–Mo ASTM-F75 alloy specimens to determine if post-manufacturing thermal treatments of an implanted material have any influence on the way protein adsorption occurs. Differences in the way in which proteins adsorb onto the surface, if they exist, would suggest that the development of the tissue/implant interface is dependent upon the metallurgical history of the alloy. Furthermore, as the tissue/implant interface develops, the way in which the alloy integrates with tissues could be influenced by post-manufacturing thermal treatments.

1.1 Adsorption and fractional coverage

In surface science fractional coverage, θ, is used to express the quantity of material adsorbed onto a surface as a function of monolayer coverage. This is the ratio between the number of occupied adsorption sites (N) to the total number of sites available for adsorption (N_s). In terms of classical surface adsorption theory it is usual to consider gas phase adsorption at constant pressure; fractional coverage can then be described by the ratio between the volume of gas adsorbed (V) relative to the volume of gas adsorbed at monolayer coverage (V_m) [12].

$$\theta = \frac{N}{N_s} = \frac{V}{V_m} \tag{1}$$

More recently adsorption from the liquid phase has been studied by constructing adsorption isotherms by measuring the amount of material retained on a surface once removed from the liquid solution. The use of XPS in this way was pioneered by Castle and Bailey [13] and was subsequently extended to ToF-SIMS by Abel et al. [14]. The experimental requirements of this approach have been reviewed by Watts and Castle [15].

In this work XPS has been used to calculate the fractional coverage based on the surface concentration of an element diagnostic of the adsorbate. There have been numerous XPS studies which have used nitrogen as a protein marker [16–18]. Chromium was used as the diagnostic substrate marker to establish the XPS signal attenuation as the adsorbed protein overlayer thickness increased. Fractional coverage was determined by quantifying the XPS spectrum and plotting the surface concentration of the adsorbate as a function of FBS concentration; this is the liquid phase/XPS version of the well known gas phase adsorption isotherm derived in the next section.

1.2 Adsorption isotherms

Adsorption is commonly described using isotherms which indicate the amount of adsorbate retained on the substrate

surface as a function of solution concentration, at a constant temperature. The kinetics of adsorption can also be studied, and consideration of both provides an indication of the kinetics and thermodynamics of the adsorption process. In practice it is usual to establish the position of kinetic equilibrium and then conduct the thermodynamic investigations.

Adsorption isotherms provide useful information regarding surface coverage and the mechanism of adsorption [16]. Adsorption can be achieved through either chemisorption or physisorption, which depends upon the type of bond formed between the adsorbate and the substrate.

Physisorption is a result of van der Waals forces which are generally long range but weak. The enthalpy of adsorption is considered to be less exothermic than -25 kJ mol^{-1}. Chemisorption is characterised by a stronger interaction between the adsorbate and substrate. Stronger secondary and even primary bonds (ionic, metallic, or covalent) are formed, generally with an enthalpy of adsorption more negative than -40 kJ mol^{-1} [15]. An important difference between the two modes of adsorption is their response to heat. Increasing the temperature will lead to a decrease in the amount of material physisorbed, but an increase in the amount of material chemisorbed, since chemisorption is an activated process. Another significant difference between physical and chemical adsorption is related to the saturation level of the adsorbed species. Chemisorption can only ever achieve monolayer formation as adsorption ceases when the adsorbate can no longer make direct contact with the substrate. However, physisorption has no such restriction and so is able to form multilayers of many molecules thick. It is possible for an initial chemisorbed layer to act as a substrate for further material to be physisorbed as described by the well-known BET isotherms.

There are many models describing chemisorption, each with different assumptions used to derive the expressions for surface coverage. Commonly used isotherms include the Langmuir, Temkin and Freundlich isotherms.

The Langmuir isotherm is the simplest isotherm and is based on the following assumptions:

- Multilayer coverage is not possible.
- All adsorption sites are equivalent.
- The probability of the adsorption of a molecule is independent of neighbouring sites being occupied or otherwise.
- The enthalpy of adsorption remains constant as a function of fractional coverage (θ).

Using these assumptions the fractional monolayer coverage, (θ), in gas phase adsorption studies at pressure, (P), can be expressed as follows:

$$\theta = \frac{bP}{1 + bP} \tag{2}$$

where b is the ratio of the rate constants for adsorption and desorption and is related to both the enthalpy of adsorption and temperature. The constant b is usually expressed as:

$$b = b_0 \exp(Q/RT) \tag{3}$$

where b_0 is a frequency factor, Q is the interaction energy, R is the gas constant and T is the temperature. Replacing σ with V/V_m (Eq. 1), Eq. 2 can be rearranged to give:

$$\frac{P}{V} = \frac{1}{bV_m} + \frac{P}{V_m} \tag{4}$$

The Temkin and Freundlich isotherms are based on the observation that the more energetically favourable sites (those with a more negative enthalpy of adsorption) are occupied first by the adsorbate. The Temkin isotherm assumes that adsorption enthalpy changes linearly with coverage. The Temkin isotherm is represented as:

$$\theta = c_1 \ln(c_2 P) \tag{5}$$

where c_1 and c_2 are constants. The Freundlich isotherm assumes that the adsorption enthalpy varies logarithmically with gas pressure and is given by:

$$\theta = c_1 P^{1/c_2} \tag{6}$$

Adsorption isotherms are expressed in the present study as the amount of adsorbate on the substrate as a function of solution concentration. For liquid phase adsorption measured using XPS the Langmuir adsorption equation can be expressed as:

$$\frac{c}{x} = \frac{1}{b\Gamma_m} + \frac{c}{\Gamma_m} \tag{7}$$

where c is the solution concentration, x is the uptake as measured by XPS and Γ_m is monolayer coverage i.e. the maximum uptake as measured by XPS. The test of conformity of experimental data to the Langmuir isotherm is achieved by plotting c/x against x. Compliance to the isotherm will result in a straight line with a gradient of $1/\Gamma_m$ and an intercept of $1/b\Gamma_m$. For liquid phase adsorption the Temkin equation 5 becomes:

$$\theta = b \ln c \tag{8}$$

and a plot of x against ln c will exhibit a straight line to show its conformity. Finally, the Freundlich isotherm is expressed as:

$$\theta = bc^{1/c_2} \tag{9}$$

Testing the conformity of experimental data to the Freundlich is achieved via a plot of log$x$ against log$c$. If the data obeys the Freundlich isotherm, a straight line will result.

Although there are many isotherms [19], the Langmuir and Temkin have been shown to be the most widely applicable in determination of adsorption isotherms by means of surface analysis [15].

2 Materials and methods

2.1 Specimen preparation

The three Co–Cr–Mo ASTM-F75 alloy samples included an AC sample, the second sample had undergone SA post-manufacture; the third had been treated by HIPing followed by SA; HIPSA. Coupons were cut from the samples with a 10 mm diameter and 2 mm thickness. Samples were polished to provide an unblemished mirror finish using a water based colloidal silica suspension with an average particle size of 0.04 μm. The polished coupons were then cleaned in an ultrasonic bath with deionized water, methanol and, finally, acetone for 5 min each. After cleaning the samples were allowed to dry in a dessicator.

2.2 Foetal bovine serum

Protein solutions were prepared using FBS (Sigma-Aldrich, Poole, UK) with a total protein content of between 4.0 and 4.3 g dL^{-1}. Solutions were made up using a serial dilution method with deionised water and FBS. A series of eight FBS concentrations varying from 100 to 10^{-5}% v/v were used. The coupons (once clean) were then placed in 5 ml of the protein solution for 30 min to allow sufficient time for adsorption to occur. Subsequently the coupons were removed from the FBS solution and were gently rinsed using Milli-Q water to ensure that any unbound proteins were removed. The same batch of FBS was used to ensure the quantity of proteins in solution was kept constant.

2.3 X-ray photoelectron spectroscopy

X-ray photoelectron spectroscopy analysis was conducted using a modified VG Scientific ESCALAB MkII electron spectrometer equipped with a Thermo Alpha 110 electron energy analyser and a Thermo XR3 digital twin anode X-ray source. The twin anode was operated using Al Kα X-ray photoelectron spectroscopy radiation at 300 W. Survey spectra over 0–1,350 eV were obtained using a pass energy of 50 eV while high resolution spectra were obtained using a pass energy of 20 eV. The control of the spectrometer and subsequent data processing was carried out using the manufacturer's software, Avantage (Ver. 4.37). For quantification, a Shirley background was subtracted from the spectra. To reduce damage due to the radiant heat from the twin anode to the delicate adsorbed proteinaceous layer the X-ray photoelectron spectroscopy source was operated 30 mm from the sample surface. For a given FBS concentration three identical samples were prepared and analysed in order to ensure repeatability. The average value obtained from three samples was used to plot the adsorption isotherms.

3 Results

Figure 1 shows the XPS survey spectrum from a polished AC Co–Cr–Mo ASTM-F75 sample. As can be seen the spectrum is dominated by strong signals originating from

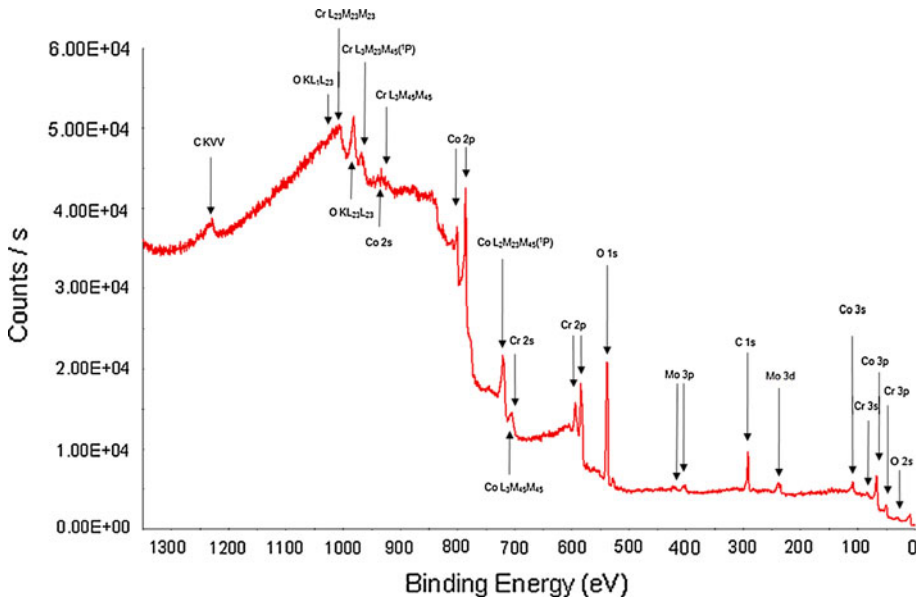

Fig. 1 XPS survey spectrum for a cleaned and polished AC sample

Table 2 Compositions of the clean Co–Cr–Mo ASTM-F75 samples

	Surface concentration, at.% (σ)				
	C	O	Cr	Co	Mo
AC	33.6 (4.7)	41.0 (3.5)	14.3 (0.4)	10.2 (2.0)	0.9 (0.5)
SA	34.3 (4.4)	40.1 (5.4)	11.7 (1.8)	13.3 (2.8)	0.6 (0.1)
HIPSA	33.8 (2.6)	38.9 (3.8)	12.5 (1.9)	14.2 (4.4)	0.6 (0.0)

C, O, Cr, Co, and Mo. The changes in the background coming from the nonelastic scattered electrons provides a non destructive means of assessing the order of the near surface layers [20]. The near horizontal background of the C, O, and the negative slope of the Cr background indicate that these are enriched on the alloys surface. The Co peak on the other hand has a positive slope indicating increased scattering due to overlayers. This suggests that the Co signal originates from a lower layer than the other peaks.

Quantitative analysis has been carried out to determine the surface composition of the three samples, the results of which are presented in Table 2.

The surface composition of all three samples have been found to be similar, with the most abundant species observed on the sample surfaces being carbon and oxygen. The significant surface concentration of carbon is adventitious contamination which may have come from the cleaning process or adsorbed from the ambient. The shape of the high resolution spectra of the Cr2p3/2 (shown in Fig. 2) is composed of two components; the first at a binding energy of approximately 574 eV originates from the metallic chromium, the second at a binding energy of 577 eV originates from chromium oxide [21]. The alloys' passive chromium oxide surface accounts for the high levels of oxygen detected.

As previously mentioned, the presence of nitrogen was assumed to be indicative of the presence of adsorbed proteins. Nitrogen is absent in the spectra taken from all three polished and clean samples. However, as shown in Fig. 3, it is present in the XPS survey spectrum taken from an AC sample immersed in 100% v/v FBS for 30 min. Comparing this survey spectrum to the spectra of the clean surface (Fig. 1) it can be seen that the Co and Cr peaks are almost lost in the background signal. The increasing background signal of the two metal peaks is a result of signal attenuation due to the proteinaceous overlayer. The horizontal background of the C, O, and N peaks shows that these signals are coming from the sample surface. Figure 4 shows the superimposed high resolution spectra of the N1s peaks after immersion in various FBS concentrations plotted against relative intensity. This shows how the N1s peak increases in intensity with increasing FBS concentrations.

The concentrations of both nitrogen and chromium on the three Co–Cr–Mo ASTM-F75 sample surfaces immersed in increasing FBS strengths are shown in Figs. 5, 6, and 7, respectively. The concentration of nitrogen is used to detect protein uptake on the sample surface, whereas the surface concentration of chromium is an attenuation plot used as a means to cross check the nitrogen isotherm.

The data shows that a plateau is reached for all three samples (for both nitrogen and chromium) and protein

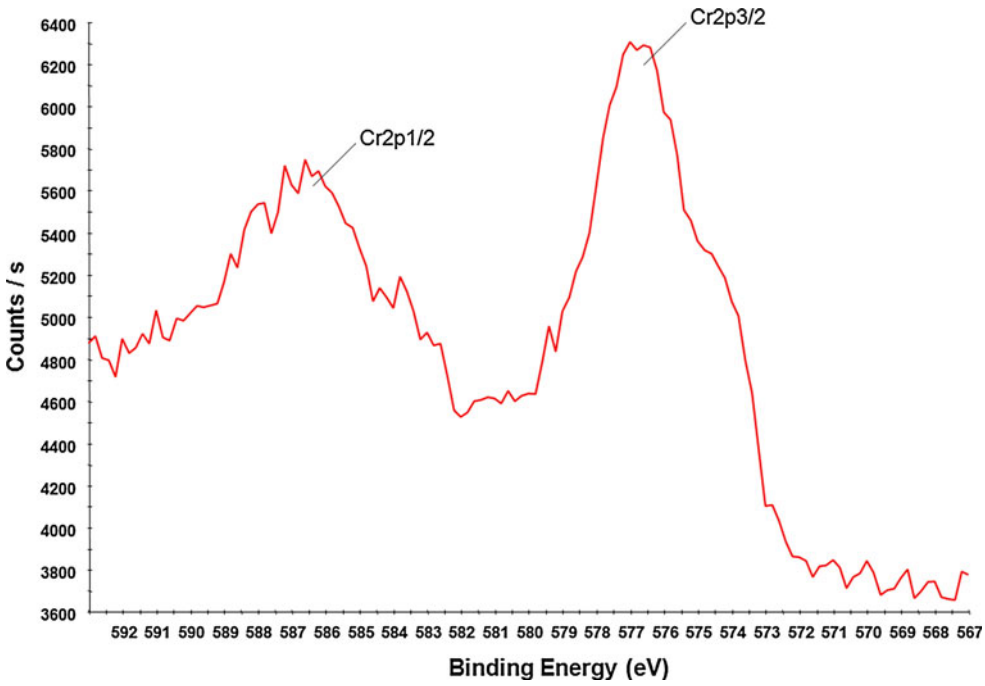

Fig. 2 High resolution fitted XPS spectra of Cr2p region

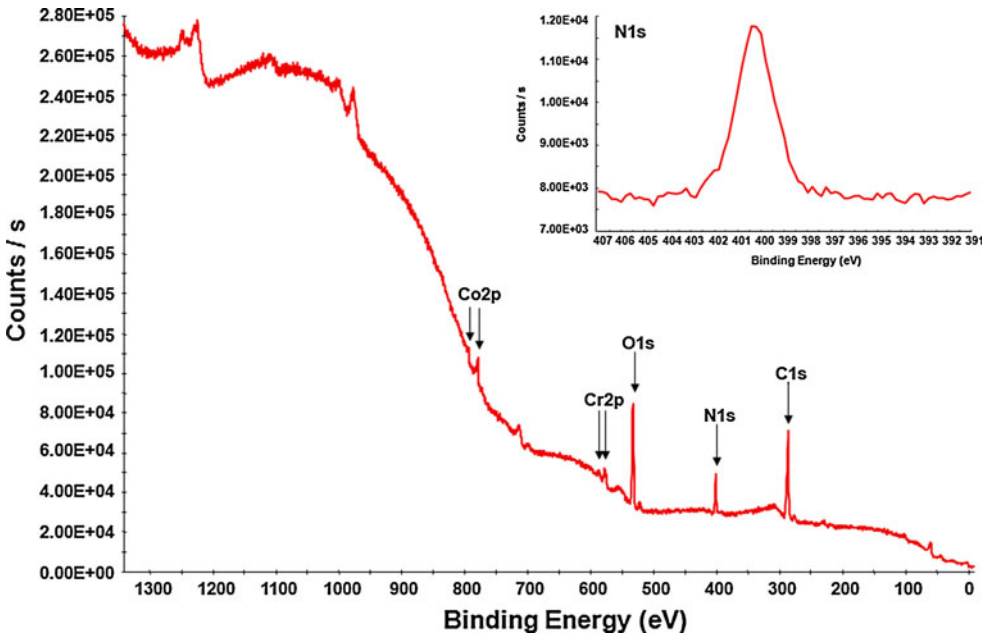

Fig. 3 XPS survey spectrum for AC sample in 100% v/v FBS

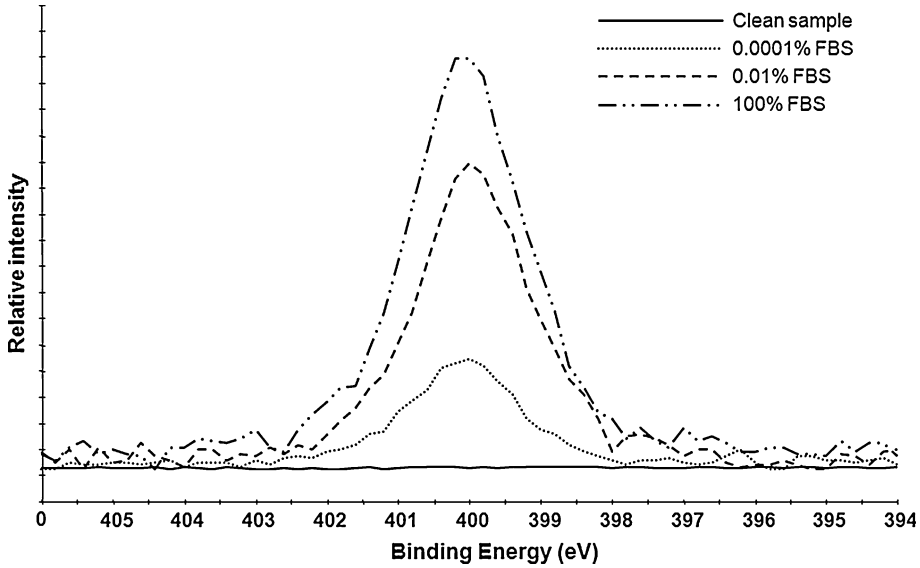

Fig. 4 XPS spectra from N1s region showing the relative nitrogen intensities obtained after immersion in a series of FBS concentrations

uptake no longer increases as a function of FBS concentration. At this point, monolayer coverage has been reached, indicating that chemisorption has occurred. The point at which a monolayer develops is known as the critical saturation of protein, and is approximately 10% v/v FBS for all three samples. The nitrogen isotherm and chromium attenuation isotherm pairs for each of the three samples are in good agreement with one another—this is verified by the fact that all three nitrogen and chromium isotherm pairs indicate monolayer coverage at the same concentration.

4 Discussion

Fractional coverage based on the averaged surface concentration of nitrogen at monolayer is shown for all three samples in Fig. 8. The data has been presented in Fig. 8 using both a linear and logarithmic scale. Conventionally linear scales are used to present adsorption isotherms as the concentration ranges studied are relatively small. However, if a much larger concentration range is used (as it is in this investigation) important attributes of the isotherm at lower concentrations are lost. So therefore the use of a

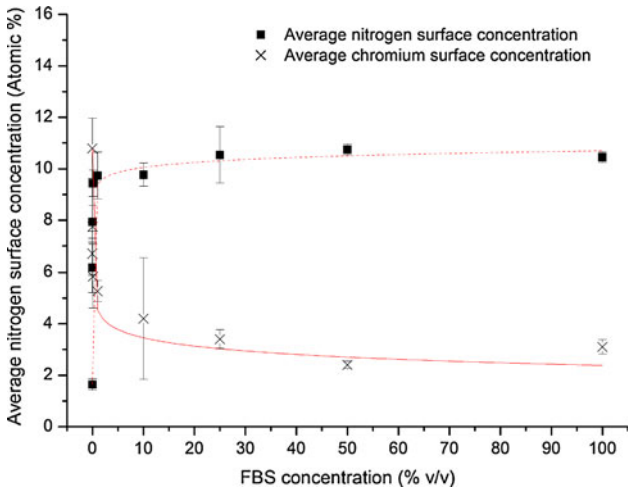

Fig. 5 Surface concentrations of nitrogen and chromium as a result of protein adsorption on the AC sample, plotted as a function of FBS concentration

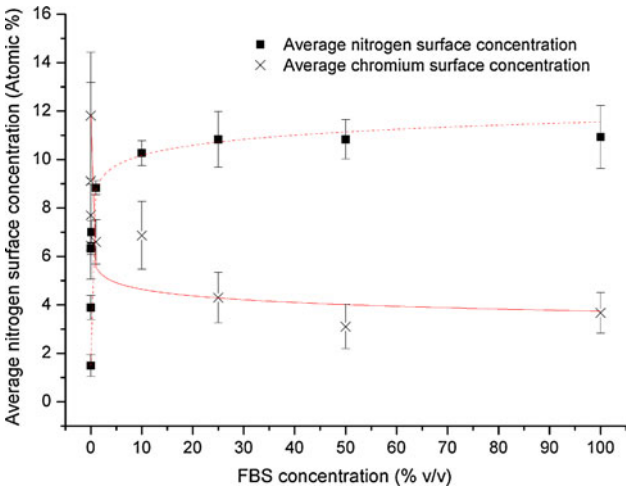

Fig. 7 Surface concentrations of nitrogen and chromium as a result of protein adsorption on the HIPSA sample, plotted as a function of FBS concentration

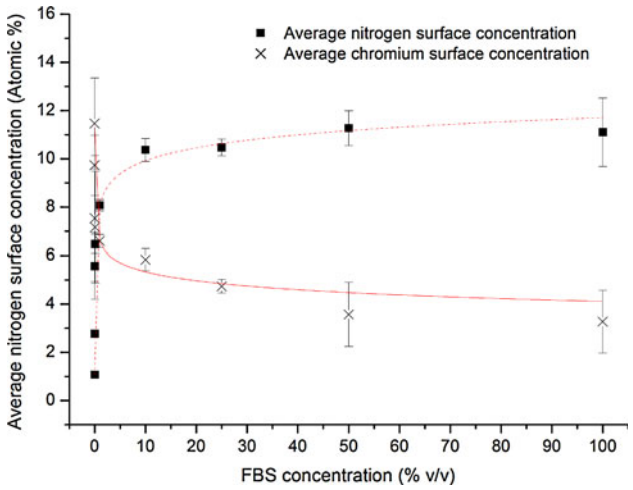

Fig. 6 Surface concentrations of nitrogen and chromium as a result of protein adsorption on the SA sample, plotted as a function of FBS concentration

logarithmic scale enables the data points at the low concentrations of the isotherm to be examined and compared. All three samples begin at a similar level of coverage and as the FBS concentration is increased develop higher levels of protein coverage. Pre monolayer coverage, the AC sample shows higher levels of protein uptake than either of the heat treated samples. The two heat treated samples both show remarkably similar levels of coverage over the concentration range used. As can be seen the AC sample reaches near monolayer coverage at much lower FBS concentrations (approx. 0.1% v/v).

The estimation of coverage based on the surface concentration of chromium is shown for all three samples in Fig. 9. The AC sample shows a higher level of coverage

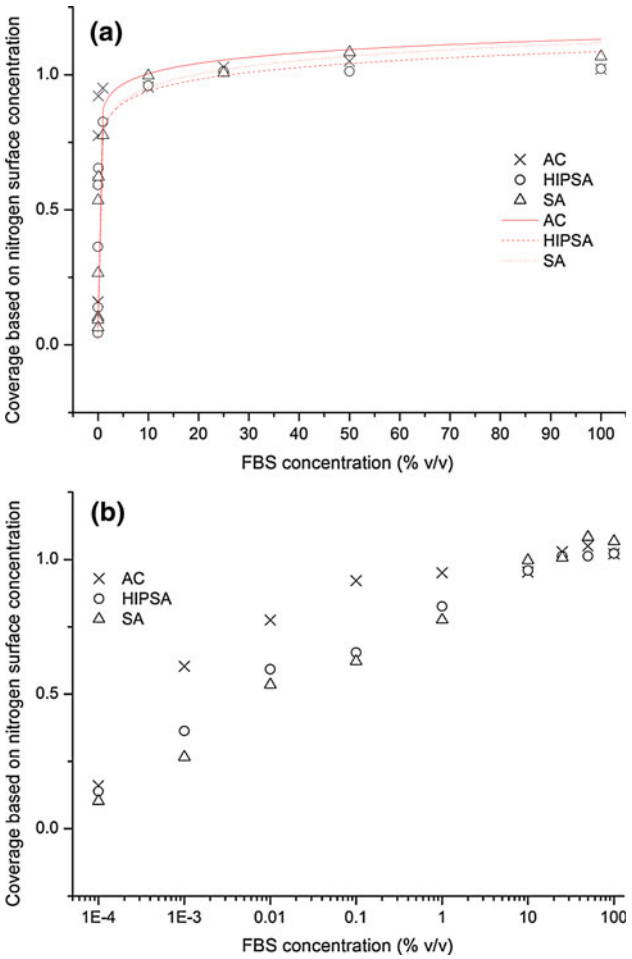

Fig. 8 Adsorption isotherms based on the surface concentration of nitrogen presented on **a** linear scale and **b** logarithmic scale

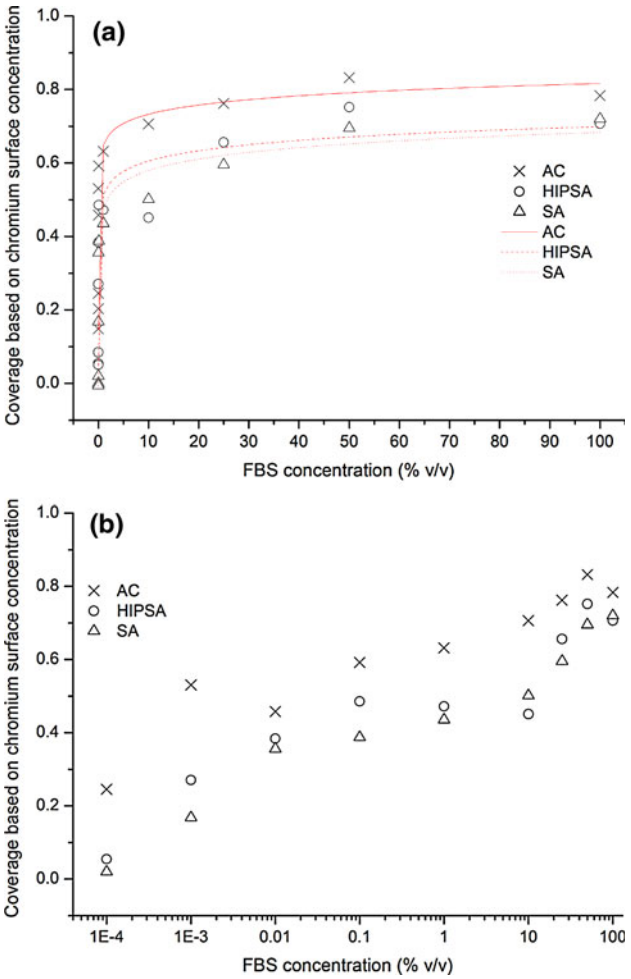

Fig. 9 Adsorption isotherm based on the surface concentration of chromium presented on **a** liner scale and **b** logarithmic scale

Table 3 Comparison of the least square values (R^2) for isotherms fitted to the Langmuir, Temkin, and Freundlich model isotherms

	R^2 for Langmuir	R^2 for Freundlich	R^2 for Temkin
AC	1.00	0.63	0.80
SA	1.00	0.86	0.98
HIPSA	1.00	0.84	0.84

than both the SA and HIPSA samples. As before, the SA and HIPSA samples are showing similar levels of coverage over the concentration range used.

From the lowest concentration used up to 10% v/v FBS (the concentration at which critical protein saturation occurs) the experimental data for all three samples have been tested for its conformity to the Langmuir, Temkin, and Freundlich isotherms. The isotherm plots were fitted with a linear line and the least square regression values (R^2) were obtained. The least square values for the isotherms are compared in Table 3.

Table 4 Theoretically and experimentally derived values for b and Γ_m

	b	Γ_m, formula value (at.%)	Γ_m, experimental value (at.%)
AC	480.7	9.8	10.2
SA	14.5	10.4	10.5
HIPSA	23.9	10.3	10.7

As indicated by the R^2 values, the experimental data give a better fit to the Langmuir model than the Temkin or the Freundlich models. As previously stated, the assumptions of the Langmuir model state that the proteins are adsorbed on the Co–Cr–Mo ASTM-F75 alloy as a monolayer, all adsorption sites are equal, and the enthalpy of adsorption is constant.

The Langmuir constants have been determined and are given in Table 4. The b (Eq. 4) constant is a dimensionless quantity which is indicative of the heat of adsorption and this can be taken as an indication of the strength of interaction between the FBS proteins and the Co–Cr–Mo ASTM-F75 substrates [14, 22]. The b value for the AC sample was found to be more than 30 times higher than that for the SA sample and 20 times higher than for the HIPSA sample. This suggests that the bonds formed by the proteins present in FBS are stronger on an AC substrate rather than on a heat treated one.

The knee of the isotherms, shown in Fig. 10, also gives a qualitative indication of the interaction energy Q between the protein and the substrate [23], related to the Langmuir constant b. The knee is much sharper in the isotherm representing protein uptake on the AC sample. This suggests that the interaction between the proteins and adsorption sites on the AC sample are stronger than those present between the proteins and adsorption sites on heat

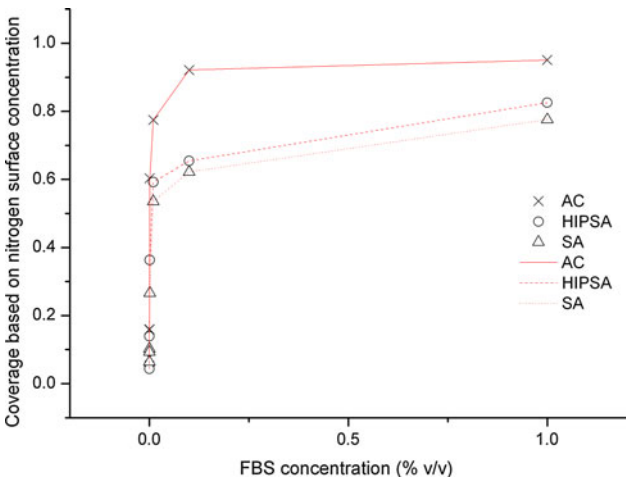

Fig. 10 Magnified portion of adsorption isotherm showing differences in 'knee' shape between the three samples

treated samples. The knees on the SA and HIPSA are both very similar. It is interesting to note that the effect of HIP does not seem to significantly alter the level of coverage seen, or the interaction energy between the proteins and the heat treated substrates.

The experimentally derived values of maximum coverage (Γ_m), Table 4, are in good agreement to those determined using the constants derived from the plots showing Langmuir conformity. This shows the applicability and accuracy of the Langmuir model to the experimental data.

The experimental data suggests that the application of post-manufacturing thermal treatments has an influence upon the adsorption of proteins on Co–Cr–Mo ASTM-F75 alloys. It is therefore possible that the way in which the three samples integrate with tissue are different. It also suggests that a different tissue/implant interface can be achieved on samples which have an identical chemistry and surface finish. The question of which of these alloys would achieve a superior tissue/implant interface will require further investigation.

The adsorption of proteins has been shown to affect not only the corrosion rate of alloys [24–27], but also form a solid lubricating layer [28–30] which is beneficial to the wear of the components. Higher levels of coverage and stronger protein/substrate interactions as seen on the AC sample would suggest that the adsorbed proteinaceous layer could be a contributing factor in the lower levels of wear seen in AC Co–Cr–Mo ASTM-F75 alloys.

5 Conclusions

Adsorption of proteins from FBS onto Co–Cr–Mo ASTM-F75 has been studied using XPS. Adsorption occurs by way of chemisorption and has been shown to obey the Langmuir model. This indicates the adsorption of a protein monolayer with a constant heat of adsorption. The bonds formed by proteins on an AC Co–Cr–Mo ASTM-F75 substrate are significantly stronger than those formed by proteins onto heat treated Co–Cr–Mo ASTM-F75 alloys.

Development of the protein conditioning layer has been shown to vary on three identical Co–Cr–Mo ASTM-F75 alloys with different metallurgical histories. This suggests that the development of the implant/tissue interface may potentially be different for all three samples; the way in which the tissue integrates with the three alloys may therefore be different. The findings of this study also seems to suggest that the HIP does not significantly alter the adsorption of proteins whereas SA has a significant impact on protein adsorption. This work warrants further investigation with other tissue constituents as the connotations could be subtle yet significant. When employing any post-manufacturing thermal treatment to a biomaterial, equal consideration should be given to the biological ramifications as that given to the material's mechanical properties.

Acknowledgments We would like to thank the EPSRC-CASE award with Smith & Nephew for the funding and supporting LAD. The authors would also like to thank Dr. Steve Hinder for his assistance with the XPS analysis.

References

1. Cawley J, Metcalf JEP, Jones AH, Band TJ, Skupien DS. A tribological study of cobalt chromium molybdenum alloys used in metal-on-metal resurfacing hip arthroplasty. Wear. 2003;255:999–1006.
2. Kamali A, Hussain A, Li C, Pamu J, Daniel J, Ziaee H, et al. Tribological performance of various CoCr microstructures in metal-on-metal bearings: the development of a more physiological protocol in vitro. J Bone Joint Surg Br. 2010;92-B:717–25.
3. Daniel J, Ziaee H, Kamali A, Pradhan C, Band T, McMinn DJW. Ten-year results of a double-heat-treated metal-on-metal hip resurfacing. J Bone Joint Surg Br. 2010;92-B:20–7.
4. Disegi JA, Kennedy RL, Pilliar R. Cobalt-base alloys for biomedical applications. West Conshohocken, PA: ASTM; 1999.
5. McMinn D. Modern hip resurfacing. London: Springer; 2009.
6. Kinbrum A, Unsworth A. The wear of high-carbon metal-on-metal bearings after different heat treatments. Proc Inst Mech Eng H. 2008;222:887–95.
7. Bowsher JG, Nevelos J, Williams PA, Shelton JC. 'Severe' wear challenge to 'as-cast' and 'double heat-treated' large-diameter metal-on-metal hip bearings. Proc Inst Mech Eng H. 2006;220:135–43.
8. Varano R, Bobyn JD, Medley JB, Yue S. The effect of microstructure on the wear of cobalt-based alloys used in metal-on-metal hip implants. Proc Inst Mech Eng H. 2006;220:145–59.
9. Tirrell M, Kokkoli E, Biesalski M. The role of surface science in bioengineered materials. Surf Sci. 2002;500:61–83.
10. Puleo DA, Nanci A. Understanding and controlling the bone–implant interface. Biomaterials. 1999;20:2311–21.
11. Kasemo B, Gold J. Implant surfaces and interface processes. Adv Dent Res. 1999;13:8–20.
12. Rattana A, Abel ML, Watts JF. ToF-SIMS studies of the adsorption of epoxy resin molecules on organosilane-treated aluminium: adsorption kinetics and adsorption isotherms. Int J Adhes Adhes. 2006;26:28–39.
13. Bailey R, Castle JE. XPS study of adsorption of ethoxysilanes on iron. J Mater Sci. 1977;12:2049–55.
14. Abel ML, Chehimi MM, Brown AM, Leadley SR, Watts JF. Adsorption-isotherms of PMMA on a conducting polymer by TOF-SIMS. J Mater Chem. 1995;5:845–8.
15. Watts JF, Castle JE. The determination of adsorption isotherms by XPS and ToF-SIMS: their role in adhesion science. Int J Adhes Adhes. 1999;19:435–43.
16. Aeimbhu A, Castle JE, Singjai P. Accounting for the size of molecules in determination of adsorption isotherms by XPS; exemplified by adsorption of chicken egg albumin on titanium. Surf Interface Anal. 2005;37:1127–36.
17. Browne MM, Lubarsky GV, Davidson MR, Bradley RH. Protein adsorption onto polystyrene surfaces studied by XPS and AFM. Surf Sci. 2004;553:155–67.
18. Sharma S, Johnson RW, Desai TA. XPS and AFM analysis of antifouling PEG interfaces for microfabricated silicon biosensors. Biosensors Bioelectron. 2004;20:227–39.
19. Bastidas DM. Adsorption of benzotriazole on copper surfaces in a hydrochloric acid solution. Surf Interface Anal. 2006;38:1146–52.

20. Watts JF, Wolstenholme J. An introduction to surface analysis by XPS and AES. New York: Wiley; 2003.
21. Salvi AM, Castle JE, Watts JF, Desimoni E. Peak fitting of the chromium 2p XPS spectrum. Appl Surf Sci. 1995;90:333–41.
22. Lowe C, Watts JF, Tegen N, Brown AM. Investigating the adsorption of components of an epoxy primer on to galvanised steel using ToF-SIMS. Surf Coat Int B-C. 2003;86:291–300.
23. Watts JF, Leadley SR, Castle JE, Blomfield CJ. Adsorption of PMMA on oxidized Al and Si substrates: an investigation by high-resolution X-ray photoelectron spectroscopy. Langmuir. 2000;16:2292–300.
24. Yan Y, Neville A, Dowson D. Biotribocorrosion—an appraisal of the time dependence of wear and corrosion interactions: II. Surface analysis. J Phys D: Appl Phys. 2006;39:3206.
25. Yan Y, Neville A, Dowson D. Biotribocorrosion of CoCrMo orthopaedic implant materials—Assessing the formation and effect of the biofilm. Tribol Int. 2007;40:1492–9.
26. Contu F, Elsener B, Bohni H. Electrochemical behavior of CoCrMo alloy in the active state in acidic and alkaline buffered solutions. J Electrochem Soc. 2003;150:B419–B24.
27. Kocijan A, Milošev I, Pihlar B. The influence of complexing agent and proteins on the corrosion of stainless steels and their metal components. J Mater Sci: Mater Med. 2003;14:69–77.
28. Serro AP, Gispert MP, Martins MCL, Brogueira P, Colaco R, Saramago B. Adsorption of albumin on prosthetic materials: implication for tribological behavior. J Biomed Mater Res A. 2006;78A:581–9.
29. Wimmer MA, Loos J, Nassutt R, Heitkemper M, Fischer A. The acting wear mechanisms on metal-on-metal hip joint bearings: in vitro results. Wear. 2001;250:129–39.
30. Tateiwa T, Clarke IC, Shirasu H, Masaoka T, Shishido T, Yamamoto K. Effect of low protein concentration lubricants in hip simulators. J Orthop Sci. 2006;11:204–11.